Conformation of an Enzyme-Bound Substrate of Staphylococcal Nuclease as Determined by NMR†

David J. Weber,‡ Gregory P. Mullen, and Albert S. Mildvan*

Department of Biological Chemistry, The Johns Hopkins University School of Medicine, 725 North Wolfe Street, Baltimore, Maryland 21205

Received March 25, 1991; Revised Manuscript Received May 14, 1991

ABSTRACT: The dinucleoside phosphodiester dTdA is a slow substrate of staphylococcal nuclease (k_{cat} = 3.8×10^{-3} s^{-1}) that forms binary E–S and ternary E–M–S complexes with Ca^{2+}, Mn^{2+}, Co^{2+}, and La^{3+}. The enzyme enhances the paramagnetic effects of Co^{2+} on $1/T_1$ and $1/T_2$ of the phosphorus and on $1/T_1$ of six proton resonances of dTdA, and these effects are abolished by binding of the competitive inhibitor 3′,5′-pdTp. From paramagnetic effects of Co^{2+} on $1/T_2$ of phosphorus, k_{off} of dTdA from the ternary E–Co^{2+}–dTdA complex is $\geq 4.8 \times 10^4$ s^{-1} and $k_{on} \geq 1.4 \times 10^6$ M^{-1} s^{-1}, indicating the $1/T_1$ values to be in fast exchange. From paramagnetic effects of enzyme-bound Co^{2+} on $1/T_1$ of phosphorus and protons, with use of a correlation time of 1.6 ps on the basis of $1/T_1$ values at 250 and 600 MHz, 7 metal–nucleus distances and 9 lower-limit metal–nucleus distances are calculated. The long Co^{2+} to ^{31}P distance of 4.1 ± 0.9 Å, which is intermediate between that expected for direct phosphoryl coordination (3.31 ± 0.02 Å) and a second sphere complex with an intervening water ligand (4.75 ± 0.02 Å), suggests either a distorted inner sphere complex or the rapid averaging of 18% inner sphere and 82% second sphere complexes and may explain the reduced catalytic activity with small dinucleotide substrates. Seventeen interproton distances and 108 lower limit interproton distances in dTdA in the ternary E–La^{3+}–dTdA complex were determined by NOESY spectra at 50-, 100-, and 200-ms mixing times. While metal–substrate and interproton distances alone did not yield a unique structure, the combination of both sets of distances yielded a very narrow range of conformations for enzyme-bound dTdA, which was highly extended, with no base stacking, with high-anti glycosidic torsional angles for dT ($64° \leq \chi \leq 73°$) and dA ($66° \leq \chi \leq 68°$) and predominantly C-2′-endo sugar puckers for both nucleosides. Although the individual nucleosides are like those of B-DNA, their unstacked conformation, which is inappropriate for base pairing, as well as the conformational angles α and γ of dA and ζ of dT, rule out B-DNA. Similarly, A- and Z-conformations are easily ruled out, providing a structural explanation of the preference of the enzyme for single-stranded DNA as substrate. While not uniquely determined by interproton distances alone, the conformation of dTdA in the binary enzyme–dTdA complex differs significantly from that found in the ternary enzyme–metal–dTdA complex. These differences were manifested directly by differing distances from $TH_{1'}$ to $TH_{4'}$, TH_6 to $TH_{2''}$, $AH_{1'}$ to $AH_{4'}$, and AH_8 to $AH_{3'}$, as well as by differing values of the conformational angles ζ and α on either side of the phosphorus of the reaction center phosphodiester, which is coordinated by the metal, and by differing values of the conformational angles γ, δ, and χ for the leaving deoxyadenosyl group. These results indicate that the metal induces conformation changes both at the attacked phosphorus and at the leaving group of the enzyme-bound substrate, which may contribute to catalysis.

Staphylococcal nuclease (EC 3.1.4.7.) is an extracellular phosphodiesterase that is activated by Ca^{2+} ions to hydrolyze phosphodiester bonds of DNA and RNA yielding 3′-mononucleotides (Tucker et al., 1979). A chemical mechanism based on the high-resolution X-ray structure of the ternary enzyme–Ca^{2+}–3′,5′-pdTp complex (Cotton et al., 1979; Loll & Lattman, 1989), extensive kinetic studies with intact and semisynthetic enzymes (Anfinsen et al., 1971; Chaiken & Sanchez, 1972), and kinetic and magnetic resonance studies of a large series of active site mutants (Serpersu et al., 1986, 1987, 1988, 1989; Hibler et al., 1987; Weber et al., 1990b,1991) is shown in Figure 1. In this mechanism, the essential Ca^{2+} activator is bound in a septacoordinate complex (Loll & Lattman, 1989) receiving three cis ligands from Asp-21, Asp-40, and the amide carbonyl group of Thr-41 of the enzyme as well as the 5′-phosphate of the competitive inhibitor 3′,5′-pdTp. The remaining three ligands are probably water molecules. The attacking water molecule is thought to be near Ca^{2+}, either in direct coordination or in the second sphere and also near Glu-43 to permit its carboxylate group to function as a general base (Hibler et al., 1987; Serpersu et al., 1989). Upon nucleophilic attack, the phosphodiester of the substrate is converted to the trigonal-bipyrimidal transition state, stabilized by Arg-87 (Serpersu et al., 1987; Weber et al., 1990b), which also acts as the general acid to protonate the 5′-oxygen of the leaving nucleoside. Although the optimum substrate is denatured, single-stranded DNA, staphylococcal nuclease also hydrolyzes native DNA, RNA, polynucleotides, and dinucleotides, as well as chromophoric phosphodiester substrates at decreased rates (Cuatrecasas et al., 1967a, 1969; Mikulski et al., 1969).

Little is known about the conformation or interactions of

† This work was supported in part by Grant DK28616 from the National Institutes of Health to A.S.M. The 600-MHz NMR Spectrometer was supported by Grant RR03518 from the National Institutes of Health, by Grant DMB8612318 from the National Science Foundation, and by the Johns Hopkins School of Medicine.

* To whom correspondence should be addressed.

‡ Recipient of a National Institutes of Health Postdoctoral Fellowship (F32 GM13324).

0006-2960/91/0430-7425$02.50/0

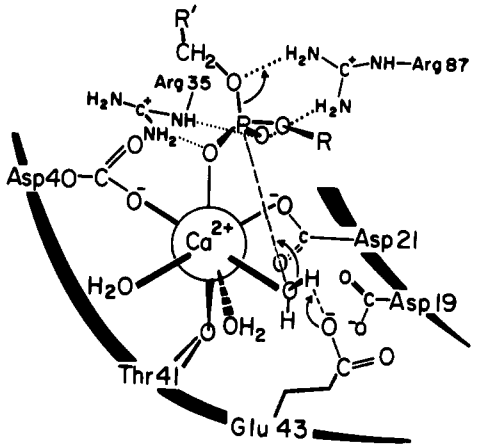

FIGURE 1: Mechanism of staphylococcal nuclease based on the 1.5-Å X-ray structure (Cotton et al., 1979), kinetic studies (Anfinsen et al., 1971), and studies of active site mutants (Serpersu et al., 1987, 1988, 1989; Hibler et al., 1987; Weber et al., 1990b, 1991) showing an additional water ligand on Ca^{2+}, as found in the refined X-ray structure (Loll & Lattman, 1989).

the enzyme-bound substrates. The conformation of the enzyme-bound inhibitor 3',5'-pdTp determined by X-ray (Cotton et al., 1979; Loll & Lattman, 1989) differs significantly from that found in solution by NMR probably due to distortion of pdTp in the crystalline state by Lys-70 and Lys-71 from a neighboring enzyme molecule in the crystal lattice (Mildvan & Serpersu, 1989; Loll & Lattman, 1989; Serpersu et al., 1989). Moreover, although 3',5'-pdTp occupies a portion of the substrate binding site in solution as shown by simple competition both in kinetic and in binding studies (Cuatrecasas et al., 1967b,c) the inhibitor interacts with the enzyme in a way different from the way authentic substrates do, as shown by differing effects of active site mutations on the affinity of the enzyme–Ca^{2+} complex for pdTp and substrates (Weber et al., 1990b, 1991).

The present paper reports for the first time the conformation of an enzyme-bound substrate on staphylococcal nuclease. The conformation of the simplest substrate, dTdA, was studied both in binary E–S and in ternary E–M–S complexes, on the basis of metal–substrate distances and interproton distances determined in solution by NMR methods. Interestingly, the conformation of enzyme-bound dTdA is found to be extended and unstacked, differing significantly from A-, B-, or Z-DNA, thus providing a structural explanation of the preference of staphylococcal nuclease for denatured single-stranded DNA. The presence of the metal significantly alters the conformation of the enzyme-bound substrate, both at the attacked phosphorus and at the leaving group, facilitating catalysis. A preliminary report of this work has been published (Weber et al., 1990a).

Materials and Methods

Materials

Solutions of nucleotides 3',5'-pdTp and dTdA (Pharmacia) were prepared, and their concentrations were determined with use of the extinction coefficients (ϵ_{260}) of 9600 and 24 600 M^{-1} cm^{-1}, respectively. Before use, buffer and nucleotide solutions were passed over Chelex 100 resin (Bio-Rad) to remove trace metals. Highly polymerized salmon sperm DNA was purchased from Sigma, and all DNA used in the enzyme assay was denatured by boiling for 30 min followed by rapid cooling on ice and passage over Chelex 100 (Cuatrecasas et al., 1967a). Isolation of wild-type staphylococcal nuclease from an engineered strain of *Escherichia coli* that carries the λ expression system and purification to homogeneity were performed as described previously (Shortle & Meeker, 1989).

Methods

Enzyme Assay. The enzymatic activity of wild-type staphylococcal nuclease was measured before and after all NMR experiments by observing the absorbance increase at 260 nm as DNA is hydrolyzed (Cuatrecasas et al., 1967a,b). Protein concentrations were determined by the absorbance at 280 nm ($\epsilon^{0.1\%} = 0.93$) at neutral pH (Dunn et al., 1973; Tucker et al., 1978, 1979) or, in the presence of nucleotides, by the method of Bradford (1976) with wild-type staphylococcal nuclease of known concentrations as the standard. The specific activity of the purified enzyme was found to be 2200 units/mg, and the enzyme retained at least 87% of its activity after prolonged NMR studies.

The activity of dTdA as a substrate of staphylococcal nuclease was determined by incubating enzyme (278 μM), $CaCl_2$ (37 mM), and dTdA (3.8 mM) in Tris-HCl, pH 7.4, for 3 h at 22 °C. Aliquots (2λ) of the solution were then applied to poly(ethyleneimine) cellulose thin-layer chromatography sheets impregnated with a fluorescent indicator (Brinkmann Instruments, Inc.). The product (50 ± 10%) was observed to separate from the unreacted substrate (50 ± 10%) with a 0.3 M $LiCl_2$ solution as the mobile phase.

Binding Studies. The concentration of free Mn^{2+} in a mixture of free and bound Mn^{2+} was determined by electron paramagnetic resonance (Cohn & Townsend, 1954) with a Varian E4 EPR spectrometer. These data were supplemented by studies of bound Mn^{2+} in the same solutions by measuring the longitudinal relaxation rates of water protons at 24.3 MHz as described previously (Mildvan & Engle, 1972) with use of a Seimco pulsed NMR spectrometer and a 180°–τ–90° pulse sequence (Carr & Purcell, 1954; Mildvan & Engle, 1972). The observed enhancement of the longitudinal relaxation rate is defined as $\epsilon^* = (1/T_{1P}^*)/(1/T_{1P})$, where $1/T_{1P}$ is the paramagnetic contribution to the relaxation rate in the presence (*) and absence of the enzyme (Mildvan & Engle, 1972). The stoichiometry of Mn^{2+} ions bound to the wild-type enzyme (n), the dissociation constant (K_D), and the enhancement of the binary complex (ϵ_b) were previously reported as were the dissociation constants of the binary enzyme–Ca^{2+} and enzyme–Co^{2+} complexes by competition with Mn^{2+} (Serpersu et al., 1986, 1989). In this study, titrations of the binary enzyme–Mn^{2+} complex with dTdA were carried out and analyzed as previously described (Reed et al., 1970; Mildvan & Engle, 1972) to yield dissociation constants and enhancement factors of ternary enzyme–Mn^{2+}–dTdA complexes. In addition, the binding of Mn^{2+} to the enzyme–dTdA complex was monitored by EPR and also by changes in T_{1P} of water protons, thereby providing the dissociation constant of Mn^{2+} from ternary enzyme–Mn^{2+}–dTdA complexes.

The dissociation constants of Ca^{2+}, Co^{2+}, and La^{3+} from their binary and ternary enzyme complexes were determined by competition with Mn^{2+}, by monitoring the bound Mn^{2+} by T_{1P} and the free Mn^{2+} by EPR, and the data were analyzed as previously described (Serpersu et al., 1986; Weber et al., 1990b, 1991).

^{31}P Relaxation Rate Measurements of dTdA. To determine the paramagnetic effects of enzyme-bound Co^{2+} on the relaxation rates of the phosphorus nucleus of dTdA bound to wild-type staphylococcal nuclease, 2.0-mL samples were prepared that contained 10 mM TES, pH 7.4, 30 mM NaCl, 20% ^2H_2O for field/frequency locking, and either 0.607 mM wild-type staphylococcal nuclease with 4.66 mM dTdA or 0.300 mM enzyme with 3.15 mM dTdA. The solutions were

Table I: Dissociation Constants (in Micromolar Concentrations) and Enhancement Factors in Binary and Ternary Enzyme–Metal, Enzyme–dTdA, and Enzyme–Metal–dTdA Complexes of Wild-Type Staphylococcal Nuclease[a]

cation	K_D	K_A'	K_S	K_3	K_2
Mn^{2+}	438 ± 22[b,c]	590 ± 58[c]	5390 ± 504	7260 ± 860	14.1 ± 4.0
Ca^{2+}	510 ± 70[b]	1780 ± 150	5390 ± 504	18810 ± 3140	42.6 ± 9.0
Co^{2+}	392 ± 63	2430 ± 70	5390 ± 504	33340 ± 6250	58.1 ± 14
La^{3+}	152 ± 15	129 ± 33	5390 ± 504	4574 ± 1310	3.09 ± 1.0

[a] The dissociation constants of the ternary and of the relevant binary complexes of enzyme (E), metal (M), and ligands (L) are defined as follows (Mildvan & Cohn, 1966): K_1 = [M][L]/[M-L]; K_D = [E][M]/[E–M]; K_2 = [E][M–L]/[E–M–L]; K_A' = [E–L][M]/[E–M–L]; K_3 = [E–M]-[L]/[E–M–L]; K_S = [E][L]/[E–L]. Note that $K_1K_2 = K_3K_D = K_A'K_S$. For dTdA, K_1 = 0.225 M is estimated on the basis of measurements of Mn^{2+}–ApU (Bean et al., 1977). [b] The stoichiometry for Mn^{2+} binding in the binary E–Mn^{2+} complex is 0.98 ± 0.06 (Serpersu et al., 1986). [c] The value is an average of titrations measuring EPR and $1/T_{1P}$ of water protons. The stoichiometry for Mn^{2+} binding in the ternary E–Mn^{2+}–dTdA complex is 0.95 ± 0.12.

then titrated with $CoCl_2$, and the increases in the longitudinal ($1/T_1$) and transverse ($1/T_2$) relaxation rates of the phosphorus resonance of dTdA were measured. Following the titration with $CoCl_2$, dTdA was displaced from the ternary enzyme–Co^{2+}–dTdA complex by the potent competitive inhibitor 3′,5′-pdTp, permitting measurement of the residual outer sphere effects on $1/T_1$ and $1/T_2$ of dTdA.

^{31}P NMR spectra were obtained at 101.25 MHz as previously described, using 12-bit analog to digital conversion, collecting 16K data points over a spectral width of 5000 Hz with an acquisition time of 1.638 s. Routine spectra were acquired by collecting 16 transients, with an 18-s delay to obtain fully relaxed spectra (>5 T_1). The longitudinal relaxation rates ($1/T_1$) of the ^{31}P resonance were measured by the nonselective saturation–recovery method, which permitted shorter recycle times. Transverse relaxation rates ($1/T_2$) were determined from the widths of resonances at half-height ($\Delta\nu_{1/2}$), where $1/T_2 = \pi\Delta\nu_{1/2}$.

The paramagnetic effects on dTdA were analyzed by plotting the increases in the relaxation rates as a function of Co^{2+} concentration. Subtracting the residual outer sphere effect measured after displacing dTdA with 3′,5′-pdTp yielded the observed $1/T_{1P}$.

The relaxation rates of dTdA resulting from Co^{2+} bound in the ternary complex were then calculated and also corrected by subtraction of the small paramagnetic effects in the residual binary Co^{2+}–dTdA complex that was also present, by utilizing the equation $(1/T_{1P})_{obs} = (MS/S_T)(1/fT_{1P})_b + (EMS/S_T)-(1/fT_{1P})_{corr}$ to solve for $(1/fT_{1P})_{corr}$. In this equation, MS, EMS, and S_T are the concentrations of the binary metal–substrate complex, the ternary enzyme–metal–substrate complex, and the total substrate, respectively. The substrate dTdA alone was titrated with Co^{2+}, and the increase in $1/T_1$ of the phosphorus resonance of dTdA was measured to obtain $(1/fT_{1P})_b$, the relaxation rate of the binary Co^{2+}–dTdA complex. The concentrations of Co^{2+}–dTdA and of enzyme–Co^{2+}–dTdA were computed by use of the measured dissociation constants for the relevant binary and ternary complexes (Table I).

Proton Relaxation Rate Measurements of dTdA. To determine the paramagnetic effects of enzyme-bound Co^{2+} on the relaxation rates of the proton resonances of dTdA bound to wild-type staphylococcal nuclease, 0.5-mL samples were initially prepared in H_2O containing 1.3 mM deuterated Tris-HCl, pH 7.4, 40.0 mM NaCl, 15.0 mM dTdA, and 1.0 mM wild-type staphylococcal nuclease. The samples were deuterated by lyophilization twice and the addition of ^2H_2O, and the measured pH was adjusted to 7.0 (pD = 7.4) with ^2HCl or NaO^2H. The resulting solutions were titrated with $CoCl_2$, and the increases in the longitudinal ($1/T_1$) and transverse ($1/T_2$) relaxation rates of the proton resonances of dTdA were measured. These data were corrected for outer sphere relaxation and were analyzed as described above for phosphorus to obtain $(1/fT_{1P})_{corr}$ and $(1/fT_{2P})_{corr}$. The correlation time τ_c for the electron nuclear dipolar interaction in the ternary enzyme–Co^{2+}–dTdA complex was determined by measuring the frequency dependence of $(1/fT_{1P})_{corr}$ of the AH_8 proton of dTdA at both 250 and 600 MHz. Evaluation of τ_c from the frequency-dependent $1/fT_{1P}$ values was done as described earlier (Mildvan & Gupta 1978; Mildvan et al., 1979; Serpersu et al., 1989).

Proton NMR spectra at 250 or 600 MHz were obtained on Bruker AM250 and AM600 NMR spectrometers by collecting 16K data points over a spectral width of 2994 or 8064 Hz for acquisition times of 2.74 or 2.03 s, respectively. Fully relaxed spectra were obtained with an 18-s delay (>5 T_1), and 16 transients were acquired for all spectra. The longitudinal relaxation rates ($1/T_1$) of the proton resonances were measured by the nonselective saturation–recovery method, and the transverse relaxation rates ($1/T_2$) were derived from the widths of the resonances at half-height, as described for the ^{31}P studies. All proton chemical shifts are reported with respect to external DSS.

Two-Dimensional NOE Experiments. To determine interproton distances on enzyme-bound dTdA, NOESY spectra (Jeener et al., 1979; Kumar et al., 1980) were acquired at 600 MHz. The samples contained either 5.11 mM staphylococcal nuclease, 6.45 mM dTdA, 37.3 mM NaCl, 0.053 mM EGTA, and 2.24 mM Tris-DCl-d_{11}, pD 7.4, in a total volume of 0.52 mL or 4.80 mM staphylococcal nuclease, 4.15 mM $LaCl_3$, 8.95 mM dTdA, 35.0 mM NaCl, 0.05 mM EGTA, and 2.2 mM Tris-DCl-d_{11}, pD 7.4, in a total volume of 0.544 mL. Samples were examined with use of three mixing times, 50, 100, and 200 ms, and the mixing times were varied randomly up to ±10% to eliminate COSY cross-peaks. All spectra were acquired in the phase-sensitive mode with use of time-proportional phase incrementation (TPPI) (Marion & Wüthrich, 1983). Optimization of receiver phase was performed to reduce base-line roll and to minimize phase correction in F2. The parameters for acquisition of NOESY spectra included a 1.0-s relaxation delay, a 0.254-s acquisition time, an 8064-Hz sweep width, 4096 time domain data points in F2, 1024 time domain points in F1, and a filter width of 20000 Hz.

Two-dimensional NOESY data were processed both on an Aspect 3000 computer, with Bruker software, and on a Personal IRIS (Silicon Graphics, Inc.), utilizing the software FELIX (Hare, Inc.), with no significant differences. NMR data processed by Bruker software were multiplied by a $\pi/3$-shifted squared sine-bell prior to Fourier transformation in F2. Linear base-line correction in F2 was done in all cases throughout the entire spectrum, and in some slices, higher order correction was required to eliminate base-line roll. The F1 direction was Fourier transformed with zero filling to 2K points. Since volume integration capabilities were not yet available on the Bruker software, optimal slices containing dTdA cross-peaks were plotted, and the areas of the peaks were integrated by cutting and weighing after correcting for scaling

factors. The peak areas were analyzed by utilizing both an initial slope method (Wüthrich, 1986; Baleja et al., 1990) and a distance extrapolation method (Baleja et al., 1990) and compared with the reference distance ($H_{1'} \rightarrow H_{2''}$ = 2.37 Å) to obtain interproton distances.

For volume integration of NOESY cross-peaks, the NMR data were processed by the program FELIX (Hare Research, Inc.) multiplying the free induction decays by a $\pi/2$-shifted squared sine-bell, Fourier transforming in F2, and base-line correcting, utilizing first to sixth order polynomal base-line corrections in F2. The F1 direction was Fourier transformed with zero filling to 2K points and in some cases base-line corrected in a manner similar to that with the F2 data. Volume integration of the dTdA peaks was achieved by first analyzing the noise around the peak of interest. If the noise around that peak was determined to give positive and negative values of equal magnitude, the data were deemed reliable, and the peak of interest was analyzed with use of the program FELIX. If, however, the noise measured was not a random distribution of positive and negative values of equal magnitude, then the spectrum required reprocessing with particular attention given to the problematic region of the spectrum during base-line correction. Once a reliable set of volume integrals were obtained, the volume data were computed, and both volume integrals for each NOE were averaged (Andersen et al., 1989) and were further analyzed as described above for the peak areas, to give interproton distances. In almost all cases, no significant differences in interproton distances were obtained by measuring peak areas or peak volumes, as previously noted (Rosevear & Mildvan, 1989).

Modeling Studies. The conformation of enzyme-bound dTdA was initially explored by building skeletal models and adjusting them to accommodate measured distances, bond distances, and van der Waals radii. When only metal to phosphorus and metal to proton distances were utilized, four alternative structures for enzyme-bound dTdA could be built, two with the metal ion above the nucleotide and two with the metal ion below the nucleotide. It was found that only one of these four alternative conformations obtained from the metal–nucleotide distances could also accommodate the interproton distances determined by the NOE[1] method.

To independently determine the range of conformations of dTdA consistent with all of the measured distances and their errors, a computer search procedure, D-Space, was used (Hare Research, Inc.). In this approach, atomic coordinates of dTdA were initially randomized by 20-Å movements of atoms in all directions, followed by annealing in 4-dimensional space (to avoid local minima), minimizing deviations from all input distances. In a typical search, 40 structures for enzyme-bound dTdA were explored. A small subset of these 40 structures was judged to be acceptable on the basis of their consistency with all covalent constraints, van der Waals constraints, angle constraints, and the measured distances within their experimental errors.

Results and Discussion

Activity of dTdA as a Substrate for Staphylococcal Nuclease. Small phosphodiester molecules, including short oligonucleotides and dinucleotides, are known to be substrates of staphylococcal nuclease but to manifest low activity in comparison with denatured DNA (Tucker et al., 1978; Sulkowski & Laskowski, 1970; Mikulski et al., 1969; Dunn & Chaiken, 1975). Thus, the rates of hydrolysis previously reported for 1.2 mM dTdT, dCdC, and dGdG are 35.2, 1.9, and 0.19 h^{-1}, respectively at 37 °C, pH 9.0. In accord with these observations, dTdA (3.8 mM) was found, under our experimental conditions, to be hydrolyzed at a rate of 2.3 h^{-1} in the presence of nuclease (278 μM), $CaCl_2$ (37 mM), and 40 mM Tris-HCl buffer, pH 7.4, at 22 °C. The measured rate for hydrolysis of dTdA may be corrected to a V_{max} of 13.7 h^{-1} (or 3.8×10^{-3} s^{-1}) on the basis of the measured dissociation constant (K_3) of dTdA from the enzyme–Ca^{2+} complex of 18.8 mM (vide infra). Although (2.5×10^4)-fold lower than V_{max} with single-stranded DNA (Serpersu et al., 1986), V_{max} of staphylococcal nuclease with dTdA is a factor of $\sim 10^{11.6}$ above the uncatalyzed rate, indicating a high catalytic power.

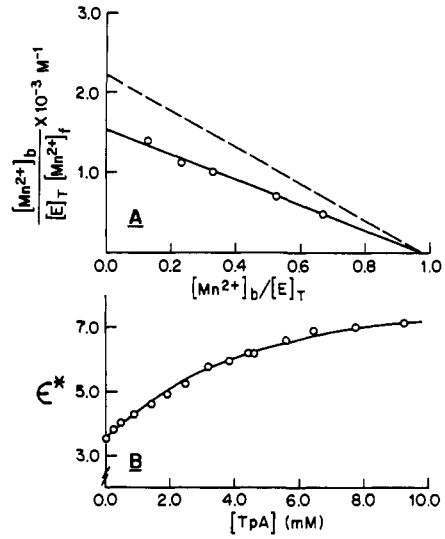

FIGURE 2: Mn^{2+} and dTdA binding by staphylococcal nuclease. (A) Scatchard plot of a titration of wild-type staphylococcal nuclease with Mn^{2+} in the presence of dTdA. The solution contained 0.670 mM wild-type staphylococcal nuclease and 7.88 mM dTdA. The dashed line is the line for a binary titration of Mn^{2+} with wild-type enzyme (Serpersu et al., 1986). (B) Titration of the enzyme–Mn^{2+} binary complex with dTdA, measuring the changes in enhancement ϵ^* of the paramagnetic effects of Mn^{2+} on $1/T_{1P}$ of water protons. The solution contained 547.5 μM wild-type enzyme with 274.1 μM $MnCl_2$. The nucleotide was added from concentrated stock solution, which also contained all other components of the titration at the same concentrations. The solid curve is computed, from the parameters given in Table I.

Thermodynamic Properties of Staphylococcal Nuclease–Metal–dTdA Complexes. The dissociation constants of the complexes studied by NMR were needed to permit quantitative interpretation of the relaxation rates of bound dTdA. The dissociation constants of Ca^{2+}, Co^{2+}, and La^{3+} from their respective binary and ternary enzyme–metal–dTdA complexes were determined by competition with Mn^{2+}, the complexes of which are easily monitored by both EPR and $1/T_{1P}$ of water protons (Serpersu et al., 1986).

(A) Titration of Enzyme–dTdA with Mn^{2+}. To determine K_A', the dissociation constant of Mn^{2+} from the ternary enzyme–Mn^{2+}–dTdA complex, nuclease was titrated with Mn^{2+} in the presence of dTdA, measuring the free Mn^{2+} concentration by EPR and the enhancement of the effect of bound Mn^{2+} on $1/T_{1P}$ of water protons. Scatchard plots of both the EPR data (Figure 2A) and the $1/T_{1P}$ data (not shown) yielded 0.95 ± 0.12 tight binding sites for Mn^{2+} with an average K_A' value of 590 ± 58 μM by the two methods (Table I).

Unlike the presence of the inhibitor 3′,5′-pdTp or the substrate 5′-pdTdA, both of which significantly raise the affinity

[1] Abbreviations: NOE, nuclear Overhauser effect; PEI, poly(ethylenimine); DSS, sodium 4,4-dimethyl-4-silapentane-1-sulfonate; EDTA, ethylenediaminetetraacetic acid; Tris-HCl, tris(hydroxymethyl)aminomethane hydrochloride

Table II: Distances from Co^{2+} to Protons and Phosphorus of dTdA in the Staphylococcal Nuclease–Co^{2+}–dTdA Complex

nucleus	δ^a (ppm)	$1/fT_{1P,corr}{}^b$ (s^{-1})	r^c (Å)	nucleus	δ^a (ppm)	$1/fT_{1P,corr}{}^b$ (s^{-1})	r^c (Å)
AH_8	8.33	647 ± 105	4.3 ● 0.90	TH_6	7.28	13.2 ± 11.4	8.2 ± 1.7
AH_2	8.18	8.0 ● 7.1	8.9 ± 1.8	TCH_3	1.83	≤53	≥5.1
$AH_{1'}$	6.36	≤61	≥5.0	$TH_{1'}$	5.95	≤53	≥5.2
$AH_{2'}$	2.80	≤121	≥4.4	$TH_{2'}$	1.66	≤54	≥5.1
$AH_{2''}$	2.54	≤164	≥4.2	$TH_{2''}$	2.20	≤54	≥5.1
$AH_{4'}$	4.14	50 ± 7.9	6.6 ± 1.4	$TH_{3'}$	4.60	58 ± 14	6.4 ± 1.30
$AH_{5',5''}$	4.06	≤46	≥5.2	$TH_{4'}$	4.01	79 ± 14	6.1 ± 1.20
P	0.33	126.1 ± 5.0[d]	4.1 ± 0.86	$TH_{5',5''}$	3.63	≤106	≥4.6

[a] ±0.02 ppm from external DSS (protons) or from 85% H_3PO_4 in 20% ^2H_2O (phosphorus). [b] $1/fT_{1P}$ values were obtained as described in the text. [c] Distances were calculated as described in the text. The τ_c was determined as 1.6 ps as determined by the frequency dependence of $1/fT_{1P,corr}$ of AH_8 (Figure 5B). Errors in r include contributions from errors in $1/fT_{1P}$ and τ_c and on the assumption that the C values used have a g value for high-spin Co^{2+} of 4 ● 2. The C values used are 895 ± 125 for Co^{2+}–proton distances and 662 ± 93 for Co^{2+}–^{31}P interactions. Errors are shown in the absolute distances, which include a 14% contribution due to the anisotropic g values of Co^{2+} and a 5–7% contribution due to experimental errors in measurements of $1/fT_{1P}$, τ_c, and the thermodynamic parameters. If the g tensor of Co^{2+} were the same in all of the complexes, the errors in the relative distances would be 5–7%. [d] $1/T_2$ values were calculated as $\pi\Delta\nu_{1/2}$. The $(1/fT_{2P})_{corr}$ is 48 103 ± 6100 (Figure 6) as determined by a least-squares fit of $1/T_2$ vs $[Co^{2+}]$ and is corrected for binary dTdA–Co^{2+} contributions as for $(1/fT_{1P})_{corr}$. Since $1/fT_{2P,corr} \gg 1/fT_{1P,corr}$ fast substrate exchange assumptions are valid, eliminating τ_m, the lifetime of the complex, from the Solomon–Bloembergen equation for $(1/fT_{1P})_{corr}$ (Solomon & Bloembergen, 1956; Mildvan & Engle, 1972).

of Mn^{2+} for wild-type enzyme (Serpersu et al., 1986, 1987, 1989; Weber et al., 1990b, 1991), the presence of dTdA slightly lowers the affinity for Mn^{2+} as illustrated by a comparison of K_D and K_A' values (Table II, Figure 2A). The difference in binding between dTdA and 3′,5′-pdTp or 5′-pdTdA is probably due to the absence of a terminal phosphate group on dTdA, which in the case of 3′,5′-pdTp and possibly of 5′-pdTdA coordinates the metal.

(B) Displacement of Mn^{2+} by Ca^{2+}, Co^{2+}, and La^{3+} in Binary and Ternary Complexes of Staphylococcal Nuclease. The dissociation constant of the binary staphylococcal nuclease–Mn^{2+} complex has previously been found to be 438 ± 22 μM by EPR and by $1/T_{1P}$ of water protons (Serpersu et al., 1986). Titrations of binary enzyme–Mn^{2+} complexes with Co^{2+} and La^{3+} and of ternary enzyme–Mn^{2+}–dTdA complexes with Ca^{2+}, Co^{2+}, and La^{3+} were carried out by measuring the decrease in $1/T_{1P}$ of water protons (Figure 3) resulting from the displacement of Mn^{2+} by the competing metal, as independently observed by EPR. The results of such titrations with Co^{2+}, Ca^{2+}, and La^{3+} indicate (Figure 3, Table I) that in all cases the metal ions compete for a single common site in both binary and ternary complexes as previously found for other nuclease complexes of Ca^{2+}, Mn^{2+}, and Co^{2+} (Serpersu et al., 1986, 1987, 1989). The affinities for metal ion binding in the binary enzyme–metal complexes are quite similar, varying only 3.3-fold from the weakest Ca^{2+}–enzyme complex to the strongest La^{3+}–enzyme complex. However, the dissociation constants of metal ions from the ternary enzyme–metal–dTdA complexes differ significantly, varying by as much as 18.8-fold in affinity, when the ternary complexes with La^{3+} and Co^{2+} are compared (Table I).

The catalytically active enzyme–Ca^{2+}–dTdA complex was shown to bind Ca^{2+} 13.8-fold weaker than La^{3+} when the respective K_A' values are compared (Table II, Figure 3). During the course of these titrations with Ca^{2+}, less than 5% of the dTdA was hydrolyzed, as determined by thin-layer chromatography.

(C) Titration of Enzyme–Mn^{2+} with dTdA. To determine K_3, the dissociation constant of dTdA from the ternary enzyme–Mn^{2+}–dTdA complex, solutions of enzyme and Mn^{2+} were titrated with dTdA and changes in enhancement (ϵ^*) of $1/T_{1P}$ of water protons (Serpersu et al., 1986; Mildvan & Engle, 1972) were measured. Such titrations, fit by computed curves (Figure 2B), yielded average K_3 values for dTdA given in Table I. The computer fitting of the nucleotide titrations also required values for K_s, the dissociation constant of the binary enzyme nucleotide complex. Although determined

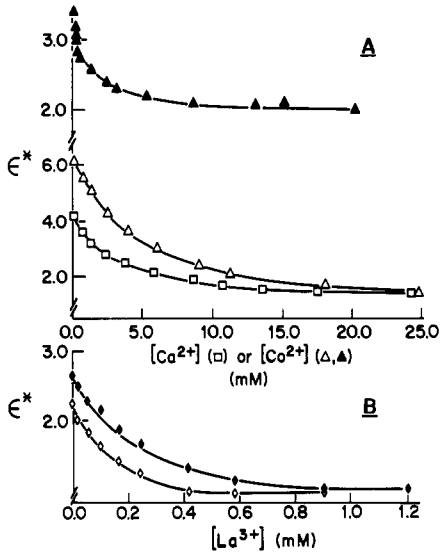

FIGURE 3: Displacement of Mn^{2+} by Ca^{2+}, Co^{2+}, or La^{3+} from binary and ternary complexes of staphylococcal nuclease monitored by changes in enhancement (ϵ^*) of the effects of Mn^{2+} on $1/T_1$ of water protons. (A) Displacement of Mn^{2+} by Ca^{2+} (□) from ternary enzyme–Mn^{2+}–dTdA complex and displacement of Mn^{2+} by Co^{2+} from binary enzyme–Mn^{2+} (▲) and ternary enzyme–Mn^{2+}–dTdA complex (△) of wild-type staphylococcal nuclease. The solutions contained 277.5 μM wild-type enzyme with 112.7 μM $MnCl_2$ and 3.81 mM dTdA (□), 246.4 μM wild-type enzyme and 178.3 μM $MnCl_2$ (▲), and 670 μM wild-type enzyme with 237.3 μM $MnCl_2$ and 7.85 mM dTdA (△). (B) Displacement of Mn^{2+} by La^{3+} from binary (◆) and ternary enzyme–Mn^{2+}–dTdA (◇) complexes of wild-type staphylococcal nuclease. The solutions contained 196.4 μM enzyme with 86.0 μM $MnCl_2$ and 2.26 mM dTdA (◇) and 261.9 μM enzyme and 129 μM $MnCl_2$ (◆). In the Co^{2+} titrations the solutions contained 40 mM TES–Na^+, pH 7.4, and in all other titrations solutions contained 40 mM Tris-HCl, pH 7.4. For all titrations the competing metal ion (Co^{2+}, Ca^{2+}, or La^{3+}) was added from concentrated stock solutions that also had the other components of the titration at the same final concentrations. In both (A) and (B), the data points are shown together with best-fit K_{app} curves. The relationship $K = K_{app}/(1 + [Mn^{2+}]/K^{Mn^{2+}})$ is utilized where K is the calculated dissociation constant for Ca^{2+}, Co^{2+}, or La^{3+} from the binary or ternary complex and $K^{Mn^{2+}}$ is the previously measured binary or ternary dissociation constant for Mn^{2+} from a binary or ternary complex (Weber et al., 1990b; 1991; Serpersu et al., 1986).

indirectly by such analysis, the resulting K_s value (5390 ± 504 μM) was consistent with data from titrations at three Mn^{2+} concentrations ranging from 182.8 to 274.1 μM at a constant enzyme concentration (574 μM). By comparing K_3 and K_s, the binding of dTdA is shown to be weakened in the presence

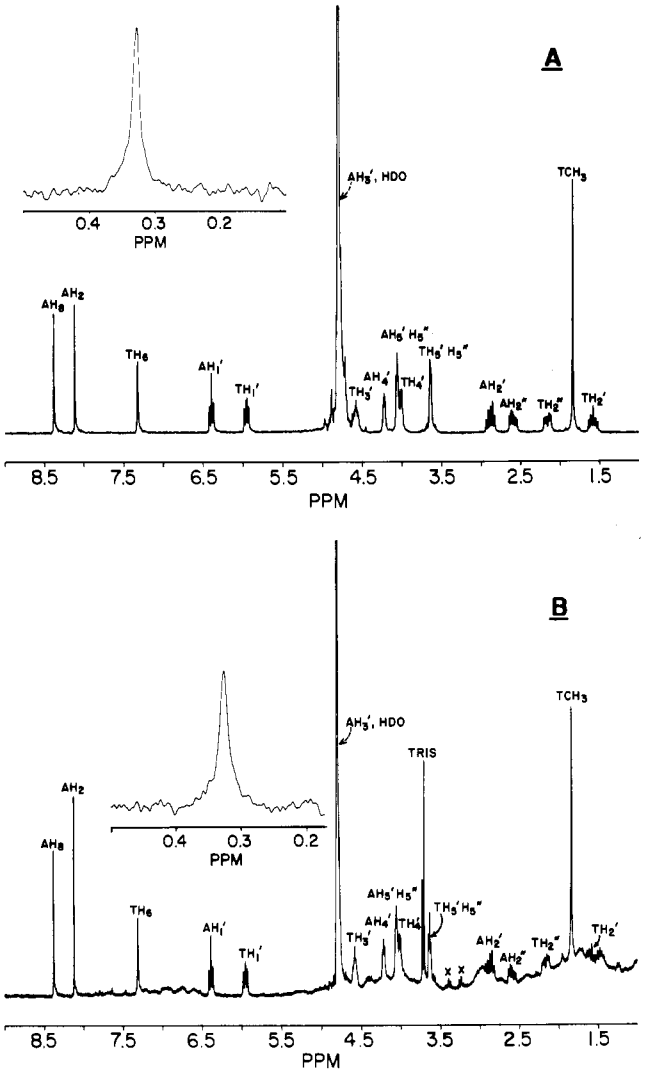

FIGURE 4: ^{31}P and ^{1}H NMR spectra of dTdA in the absence and presence of staphylococcal nuclease utilized for Co^{2+} titrations. (A) 250-MHz proton and (inset) 101.25-MHz phosphorus NMR spectrum in the absence and (B) in the presence of wild-type staphylococcal nuclease. The samples (0.5 mL) utilized for collecting proton data were prepared in D_2O that contained 1.3 mM deuterated Tris-DCl, pH 7.0 (pD = 7.4), 40 mM NaCl, and 15.0 mM dTdA in the (A) absence and (B) presence of 1.0 mM wild-type staphylococcal nuclease, $T = 25$ °C. The samples (2.0 mL) utilized for collecting phosphorus data were prepared in 20% ^2H_2O for field/frequency locking, 10 mM TES, pD 7.4, 30 mM NaCl, and 4.66 mM dTdA in the (A) absence and (B) presence of 0.607 mM wild-type staphylococcal nuclease, $T = 25$ °C. The peaks marked X are present in spectra of enzyme alone.

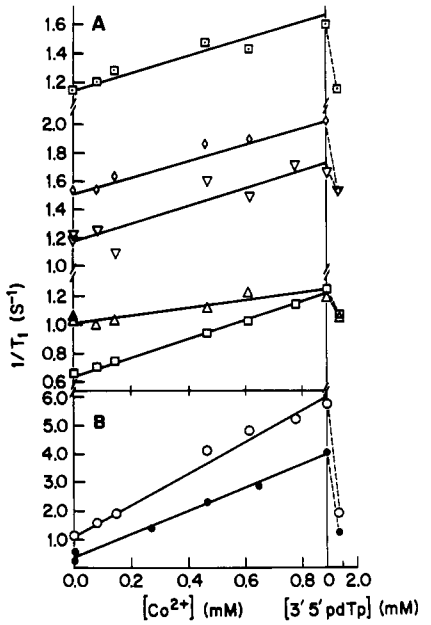

FIGURE 5: Paramagnetic effects of Co^{2+} on proton resonances of dTdA at 250 MHz and the frequency dependence of the effect on the AH_8 proton, at 250 and 600 MHz. (A) $1/T_1$ of proton resonances of dTdA vs $[Co^{2+}]$, corrected for the outer sphere contribution by displacement of dTdA from the enzyme by the competitive inhibitor 3′,5′-pdTp for the protons (□) $TH_{3'}$, (◇) $TH_{4'}$, (▽) TH_6, (△) $AH_{4'}$, and (□) AH_2 of dTdA. (B) Frequency dependence of the paramagnetic effects of Co^{2+} ions on the AH_8 proton of dTdA at 250 MHz (○) and 600 MHz (●). The solutions contained 1.0 mM wild-type enzyme, 15.0 mM dTdA, 40.0 mM NaCl, and 1.26 mM deuterated Tris-DCl, pD 7.4, 25 °C. Displacement of dTdA from the enzyme was with 3′,5′-pdTp to a final concentration of 0.91 mM.

of metal ion, a finding consistent with the weakening of Mn^{2+} binding to the enzyme by dTdA.

Paramagnetic Effects of Enzyme-Bound Co^{2+} on Relaxation Rates of Proton and Phosphorus Resonances of dTdA. *(A) Proton NMR Studies.* The ^{1}H NMR spectrum of dTdA at 250 MHz was assigned (Table II) in the absence of enzyme (Figure 4A) by utilizing standard proton decoupling, 1-D NOE, and 2-D NOE methodology. To unequivocally locate the resonances of dTdA in the presence of enzyme (Figure 4B), the spectrum of enzyme alone was subtracted from that of the enzyme–dTdA mixture (not shown) and assigned from chemical shifts relative to DSS and coupling patterns. Two-dimensional NOE data in the presence of the enzyme confirmed these assignments (vide infra).

Titrations with $CoCl_2$ measuring the $1/T_1$ of the proton resonances of dTdA in the absence or presence of wild-type staphylococcal nuclease indicate that the enzyme enhances the paramagnetic effects of Co^{2+} on $1/T_1$ of the deoxyadenosine protons of dTdA, AH_8, $AH_{4'}$, and AH_2 (Figure 5A,B), and the thymidine protons $TH_{4'}$, $TH_{3'}$, and TH_6 (Figure 5A). The enhancement factors, obtained from the ratios of slopes in the titration curves of Figure 5, were 5.95, 1.90, and 1.18 for the adenine H_8, $H_{4'}$, and H_2, respectively, and were 3.25, 2.04, and 1.22 for the thymidine $H_{4'}$, $H_{3'}$, and H_6, respectively. Displacement of dTdA from its ternary enzyme complex by the competitive inhibitor 3′,5′-pdTp abolished the paramagnetic effects on $TH_{3'}$, $TH_{4'}$, $AH_{4'}$, and AH_8 and significantly decreased the paramagnetic effects on the TH_6 and AH_2 proton resonances (Figure 5). The concentration of 3′,5′-pdTp (247 ± 10 μM) that gave half-maximal displacement of dTdA was comparable to that predicted (267 ± 30 μM) on the basis of all of the equilibrium constants for the respective ternary Co^{2+} complexes of dTdA (Table I) and 3′,5′-pdTp (Mildvan & Serpersu, 1989). With TH_6 and AH_2 the residual outer sphere contributions to the relaxation rates were thus determined and used to correct the relaxation rates for the distance calculations.

(B) Phosphorus NMR Studies. The proton-decoupled ^{31}P NMR spectrum of dTdA obtained at 101.25 MHz consists of a resonance 0.3 ppm downfield from H_3PO_4 as an external reference (Figure 4A,B inset). Titration with $CoCl_2$ in the absence (not shown) and presence of enzyme gave an enhancement factor of 3.2 for the paramagnetic effect of Co^{2+} on the $1/T_1$ of the phosphorus resonance and an enhancement factor of 4.0 on $1/T_2$ (Figure 6). As in the proton NMR studies, all Co^{2+} titrations were followed by the displacement of dTdA by the inhibitor 3′,5′-pdTp, which revealed no residual outer sphere contributions to the relaxation rates of phosphorus. The concentration of 3′,5′-pdTp (60 ± 10 μM) that

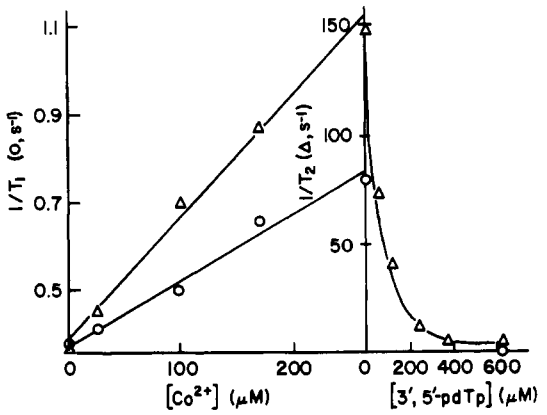

FIGURE 6: Paramagnetic effects of Co^{2+} on $1/T_1$ (O) and $1/T_2$ (Δ) of the phosphorus resonance of dTdA at 101 MHz. The solution contained 0.607 mM wild-type staphylococcal nuclease, 4.66 mM dTdA, 30 mM NaCl, 20% ^2H_2O for field/frequency locking, and 10 mM TES-Na^+, pH 7.4, T = 25 °C. Displacement of dTdA from the enzyme was with 3′,5′-pdTp titrated to a final concentration of 0.611 mM.

gave half-maximal displacement of dTdA from the ternary enzyme–Co^{2+}–dTdA complex, as measured by the decrease in $1/T_2$ (Figure 6), was comparable to that predicted (40 ± 20 μM) on the basis of all of the equilibrium constants for the respective ternary Co^{2+} complexes of dTdA (Table I) and 3′,5′-pdTp (Mildvan & Serpersu, 1989).

Cobalt to Phosphorus and Cobalt to Proton Distances in the Ternary Enzyme–Co^{2+}–dTdA Complex. The concentrations of Co^{2+} in the binary Co^{2+}–dTdA and ternary enzyme–Co^{2+}–dTdA complexes were calculated from the six dissociation constants (Table II), permitting an evaluation of the normalized relaxation rates $(1/fT_{1P})_{corr}$ and $(1/fT_{2P})_{corr}$ for the protons and phosphorus in each ternary complex (see Methods). The $(1/fT_{2P})_{corr}$ value for phosphorus (4.8×10^4 s^{-1}, Table II) sets a lower limit to the rate constant for dissociation of dTdA from the ternary complex. From this value and from K_3 (Table I), a lower limit of 1.4×10^6 M^{-1} s^{-1} for the rate constant for binding of dTdA is obtained. These values, which are several orders of magnitude greater than all of the values of $(1/fT_{1P})_{corr}$, establish the latter to be in the fast-exchange limit (Mildvan & Engle, 1972; Mildvan & Gupta, 1978). Thus, the values of $(1/fT_{1P})_{corr}$ are the paramagnetic effects of Co^{2+} on dTdA in the ternary complex and are therefore suitable for distance calculations. The remaining parameter required for distance calculations, the correlation time (τ_c), was determined from the frequency dependence of $(1/fT_{1P})_{corr}$ of the AH_8 proton at 250 and 600 MHz (Mildvan & Engle, 1972; Serpersu et al., 1988) (Figure 5B). From the experimental ratio fT_{1P}(600 MHz)/fT_{1P}(250 MHz) of 1.415 ± 0.020, a correlation time τ_c of 1.64 ± 0.06 ps was calculated, assuming τ_c to be independent of frequency over this range. The alternative assumption, that τ_c showed a maximal frequency dependence over this range, was inconsistent with the measured fT_{1P} ratio. This correlation time, which represents the longitudinal electron spin relaxation time of Co^{2+}, was used to calculate all of the distances. In cases where enhancements were not detected, lower limit distances were calculated from an analysis of the error levels of the titration $(1/fT_{1P})_{corr}$ and of the outer sphere contribution $(1/T_{1os})$.

The Co^{2+} to phosphorus distance (4.1 ± 0.9 Å) lies between that expected for direct phosphate coordination (3.31 ± 0.02 Å) and a second sphere complex with an intervening water ligand (4.75 ± 0.02 Å) (Serpersu et al., 1989). The mean value of 4.1 Å is consistent with either a distorted inner sphere phosphoryl complex or the rapid averaging of 18% inner sphere and 82% second sphere coordination. This long metal to phosphorus distance may explain the reduced catalytic activity of staphylococcal nuclease with small substrates (Tucker et al., 1978).

With seven measured distances from Co^{2+} to dTdA ranging from 4.1 to 8.9 Å (Table II) and nine lower limit distances, four stick models, all with extended conformations, could be constructed, two with the Co^{2+} ion above the bridging phosphorus and two with the Co^{2+} ion below the phosphorus.

In these four structures, significant differences were noted in the glycosidic torsional angles of dTdA in both the purine and pyrimidine nucleotides. Since glycosidic torsional angles are well determined by measurements of interproton distances by the nuclear Overhauser effect (Rosevear & Mildvan, 1989), ambiguities in the conformation of enzyme-bound dTdA were resolved by this method.

Intramolecular Nuclear Overhauser Effects on Enzyme-Bound dTdA. The stable ternary enzyme–La^{3+}–dTdA complex was studied because La^{3+} is diamagnetic, occupies the Ca^{2+} site, and does not activate hydrolysis. Parts A and B of Figure 7 show selected portions of a phase-sensitive NOESY spectrum of enzyme, La^{3+}, and dTdA at 600 MHz with a mixing time of 50 ms. Typical slices from this NOESY experiment are also displayed (Figure 7C,D) to show the quality of the data. In the first case (Figure 7C), the AH_8 proton resonance of enzyme-bound dTdA is on the diagonal, giving rise to the negative NOE's displayed, while in the second case (Figure 7D), the TH_6 proton of enzyme-bound dTdA is on the diagonal.[2] The negative intramolecular NOE's of dTdA establish these to come from the enzyme-bound substrate. In the absence of enzyme, the NOESY experiments give only positive NOE's (not shown), as is generally observed for small molecules (Rosevear et al., 1983). This point was independently confirmed in displacement experiments with 3′,5′-pdTp, which eliminated the negative NOE's of dTdA. Negative NOE's from enzyme-bound 3′,5′-pdTp then appeared. However, at the conditions used to observe the negative NOE's resulting from bound 3′,5′-pdTp, positive NOE's from free dTdA cannot be observed, as previously found for mononucleotides (Ferrin & Mildvan, 1985).

To accurately determine interproton distances, NOESY spectra were collected at three mixing times (50, 100, and 200 ms) to obtain NOE buildup curves, which were analyzed by two independent methods (Table III). In the first method, the initial slope of the NOE buildup was compared to that of a standard NOE between protons at a known distance, i.e., $H_{1'} \rightarrow H_{2''}$ at 2.37 Å. Distances were calculated with use of the relationship $r = 2.37/(\sigma_{x,x}/\sigma_{H1',H2''})^{1/6}$ where $\sigma_{H1',H2''}$ and $\sigma_{x,x}$ are the initial slopes calculated from a least-squares fit of the lines through the NOE buildup of the standard and NOE of interest, respectively (Table III). In cases where there is significant deviation from the initial slope at 200 ms ($TH_6 \rightarrow TH_{2'}$, $AH_8 \rightarrow AH_{2'}$, $H_{1'} \rightarrow H_{2''}$), only the 50-ms and 100-ms points were used as previously suggested (Wüthrich, 1986; Baleja et al., 1990).

In the second method (Table III), a distance is calculated at each mixing time (50, 100, or 200 ms) relative to a standard ($H_{1'}$ to $H_{2''}$ = 2.37 Å) with use of $r = 2.37/(I_{x,x}/I_{H1',H2''})^{1/6}$ where $I_{H1',H2''}$ and $I_{x,x}$ are the intensities of the standard and NOE of interest, respectively, at the same mixing time. The calculated distances were plotted versus mixing time and ex-

[2] In addition to the intramolecular NOEs in enzyme-bound dTdA, intramolecular enzyme to enzyme NOEs, and intermolecular enzyme to dTdA NOEs were observed. These will be discussed in a future publication.

Table III: Interproton Distances Calculated from NOESY Data of dTdA in the Ternary Enzyme–La^{3+}–dTdA Complex of Staphylococcal Nuclease

proton pair B → A[a]	distances from volume integration[b] method 1 (initial slope)[c]	method 2 (r vs mixing time)[b,d]	average	distances from optimal slice area integration[e] average
$TH_{1'} \rightarrow TH_{4'}$	3.03 ± 0.17	3.18 ± 0.33	3.11 ± 0.37	2.96 ± 0.32
$TH_{1'} \rightarrow TH_{2''}$	2.37 ± 0.10[f]	2.37 ± 0.10[f]	2.37 ± 0.10[f]	2.37 ± 0.10[f]
$TH_{1'} \rightarrow TH_{2'}$	2.80 ± 0.06	3.05 ± 0.10	2.93 ± 0.12	2.90 ± 0.13
$AH_{1'} \rightarrow AH_{4'}$	3.33 ± 0.23	3.18 ± 0.10	3.26 ± 0.28	3.17 ± 0.21
$AH_{1'} \rightarrow AH_{2''}$	2.37 ± 0.10[f]	2.37 ± 0.10[f]	2.37 ± 0.10[f]	2.37 ± 0.10[f]
$AH_{1'} \rightarrow AH_{2'}$	2.85 ± 0.19[g]	2.95 ± 0.19[g]	2.90 ± 0.27[g]	2.92 ± 0.25[g]
$TH_6 \rightarrow TH_{1'}$	2.91 ± 0.38	2.88 ± 0.28	2.90 ± 0.47	2.94 ± 0.26
$TH_6 \rightarrow TH_{5'}H_{5''}$	4.32 ± 0.40	4.05 ± 0.58	4.19 ± 0.73	3.67 ± 0.39
$TH_6 \rightarrow TH_{2''}$	3.31 ± 0.33	3.11 ± 0.44	3.21 ± 0.55	3.31 ± 0.47
$TH_6 \rightarrow TCH_3$	2.91 ± 0.17[h]	2.87 ± 0.08[h]	2.89 ± 0.19[h]	2.94 ± 0.11[h]
$TH_6 \rightarrow TH_{2'}$	2.10 ± 0.23	2.09 ± 0.13	2.09 ± 0.26	2.28 ± 0.12
$TH_6 \rightarrow TH_{3'}$	3.07 ± 0.19	3.28 ± 0.40	3.18 ± 0.45	3.04 ± 0.31
$AH_8 \rightarrow AH_{1'}$	3.37 ± 0.33	3.51 ± 0.21	3.44 ± 0.39	3.40 ± 0.17
$AH_8 \rightarrow AH_{5'}H_{5''}$	3.43 ± 0.24	3.47 ± 0.19	3.45 ± 0.31	3.50 ± 0.16
$AH_8 \rightarrow AH_{2'}$	2.54 ± 0.12	2.66 ± 0.11	2.60 ± 0.16	2.61 ± 0.14
$AH_8 \rightarrow AH_{2''}$	3.40 ± 0.24	3.88 ± 0.19	3.64 ± 0.31	3.52 ● 0.30
$AH_8 \rightarrow AH_{3'}$	3.60 ± 0.72	4.15 ± 0.55	3.88 ± 0.91	3.77 ± 0.20

[a] B → A represents an NOE occurring between the protons A and B as measured in both columns and rows of a two-dimensional NOESY. [b] Distances calculated for each single mixing time were based on volume integration of the NOESY cross-peaks, assuming a distance of 2.37 Å from $H_{1'}$ to $H_{2''}$ as a standard, using the formula

$$r_{B\rightarrow A} = \left(\frac{I_{H1'\rightarrow H2''}}{I_{B\rightarrow A}}\right)^{1/6} (2.37\ \text{Å})$$

where I is the average integrated volume of the NOE at the mixing time of interest. For $H_{5'}H_{5''}$ and for TCH_3 peaks $I/2$ and $I/3$ were utilized, respectively, to solve for $r_{B\rightarrow A}$. The standard values $I_{H1'\rightarrow H2''}$ utilized were $I_{200ms} = 12.19$; $I_{100ms} = 7.79$; and $I_{50ms} = 5.49$. [c] Distances calculated with use of the initial slope method were based on the formula

$$r_{B\rightarrow A} = \left(\frac{\sigma_{H1'\rightarrow H2''}}{\sigma_{B\rightarrow A}}\right)^{1/6} (2.37\ \text{Å})$$

where σ is the slope resulting from a plot of integration volume of the NOESY cross-peaks vs mixing time. The standard buildup rate value $S_{H1\rightarrow H2''}$ was 91.5 volume integral units/s. In cases where leveling occurred between 100 and 200 ms, the slope was taken from 0 to 100 ms ($AH_8 \rightarrow AH_{2'}$, $TH_6 \rightarrow TH_{2'}$, and the standard $H_{1'} \rightarrow H_{2''}$). [d] Distances, $r_{B\rightarrow A}$, calculated at each mixing time 50, 100, and 200 ms were plotted vs mixing time and extrapolated to zero mixing time to correct for spin diffusion as previously described (Baleja et al., 1990). At the lowest mixing time, 50 ms, two experimental distances were utilized. [e] For each proton pair, the area of optimal slices was taken from two-dimensional NOESY experiments at 50, 100, and 200 ms, respectively. Distances were determined by utilizing the same methods of analysis as those used for the volume integrated data, and only the final average of the two methods is shown. [f] Assumed as internal standards. [g] Expected value was 2.9 ± 0.2 Å (Rosevear et al., 1983). These results provide an internal check on the measured interproton distances. [h] Expected value was 2.9 ± 0.1 Å. These results provide an additional internal check on the measured interproton distances.

Table IV: Interproton Distances Calculated from NOESY Data of dTdA in the Binary Enzyme–dTdA Complex of Staphylococcal Nuclease

proton pair B → A[a]	distances from volume integration[b] method 1 (initial slope)[b]	method 2 (r vs mixing time)[b]	average	distances from optimal slice area integration[b] average
$TH_{1'} \rightarrow TH_{4'}$	≥4.2[c]	≥4.2[c]	≥4.2[c]	≥4.2[c]
$TH_{1'} \rightarrow TH_{2''}$	2.37 ± 0.10[d]	2.37 ± 0.10[d]	2.37 ± 0.10[d]	2.37 ± 0.10[d]
$TH_{1'} \rightarrow TH_{2'}$	3.00 ± 0.30[e]	3.00 ± 0.30[e]	3.00 ± 0.42[e]	2.91 ± 0.07[e]
$AH_{1'} \rightarrow AH_{4'}$	≥4.2[c]	≥4.2[c]	≥4.2[c]	≥4.2[c]
$AH_{1'} \rightarrow AH_{2''}$	2.37 ± 0.10[d]	2.37 ± 0.10[d]	2.37 ± 0.10[d]	2.37 ± 0.10[d]
$AH_{1'} \rightarrow AH_{2'}$	2.75 ± 0.27[e]	3.06 ± 0.28[e]	2.91 ± 0.40[e]	2.80 ± 0.18[e]
$TH_6 \rightarrow TH_{1'}$	3.05 ± 0.31	3.35 ± 0.41	3.20 ± 0.51	2.93 ± 0.30
$TH_6 \rightarrow TH_{5'}H_{5''}$	3.20 ± 0.56	3.52 ± 0.20	3.36 ± 0.59	2.91 ± 0.41
$TH_6 \rightarrow TH_{2''}$	≥4.2[c]	≥4.2[c]	≥4.2[c]	≥4.2[c]
$TH_6 \rightarrow TCH_3$	3.08 ± 0.27[f]	2.95 ± 0.15[f]	3.02 ± 0.31[f]	2.96 ± 0.23[f]
$TH_6 \rightarrow TH_{2'}$	2.10 ± 0.30	2.30 ± 0.45	2.20 ± 0.54	2.28 ± 0.21
$TH_6 \rightarrow TH_{3'}$	3.12 ± 0.38	3.52 ± 0.42	3.22 ± 0.57	2.88 ± 0.32
$AH_8 \rightarrow AH_{1'}$	3.25 ± 0.42	3.51 ± 0.30	3.38 ± 0.52	3.22 ± 0.30
$AH_8 \rightarrow AH_{5'}H_{5''}$	3.67 ± 0.20	4.00 ± 0.50	3.84 ± 0.54	3.49 ± 0.17
$AH_8 \rightarrow AH_{2'}$	2.38 ± 0.24	2.37 ± 0.10	2.37 ± 0.26	2.45 ± 0.24
$AH_8 \rightarrow AH_{2''}$	3.38 ± 0.46	3.95 ± 0.50	3.67 ± 0.68	3.84 ± 0.36
$AH_8 \rightarrow AH_{3'}$	≥4.2[c]	≥4.2[c]	≥4.2[c]	≥4.2[c]

[a] B → A represents an NOE occurring between the protons A and B as measured in both columns and rows of a two-dimensional NOESY. [b] Distances were calculated as described in Table III. [c] Lower limit distances were based on the integration of the noise of a 1-D slice or 2-D NOE experiment. [d] Assumed as internal standards. [e] Expected value was 2.9 ± 0.2 Å (Rosevear et al., 1983). These results provide an internal check on the measured interproton distances. [f] Expected value was 2.9 ± 0.1 Å. These results provide an additional internal check on the measured interproton distances.

trapolated to a distance at zero mixing time, thereby correcting for spin diffusion (Baleja et al., 1990). When the two methods are compared for both the ternary E–La^{3+}–dTdA and binary E–dTdA complexes (Tables III and IV), it is evident that mutually consistent distances are obtained by both methods. For the distance extrapolation method, it is most important

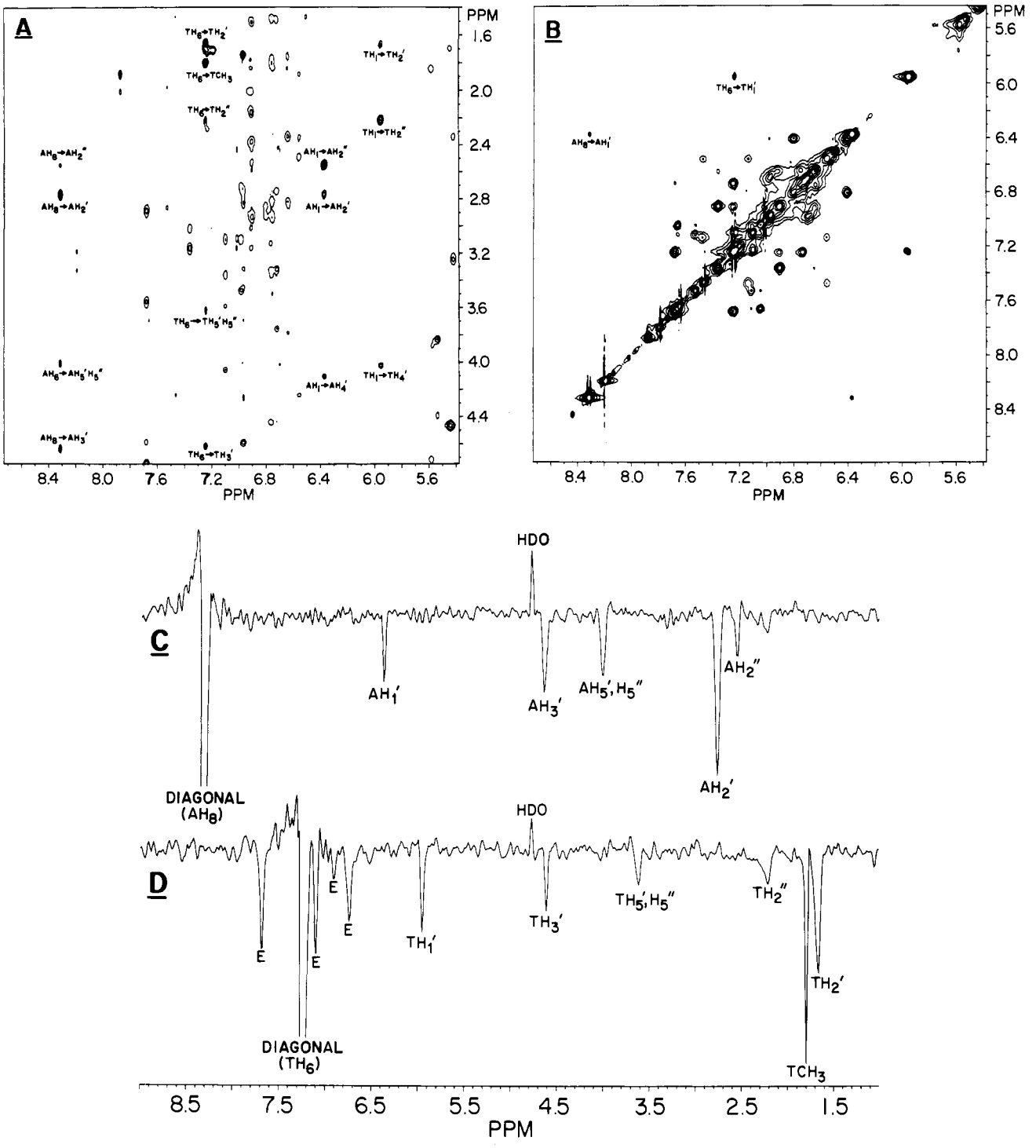

FIGURE 7: Two-dimensional nuclear Overhauser effect (NOESY) spectra at 600 MHz of the enzyme–La^{3+}–dTdA ternary complex of wild-type staphylococcal nuclease. (A) The upfield/downfield and (B) downfield regions of a 50-ms two-dimensional NOESY spectrum of the enzyme–La^{3+}–dTdA ternary complex of staphylococcal nuclease. The sample contained 4.80 mM wild-type staphylococcal nuclease, 4.15 mM $LaCl_3$, 8.95 mM dTdA, 35 mM NaCl, 0.05 mM EGTA, and 2.2 mM deuterated Tris-DCl, pD 7.4, in a total of 0.544 mL, 27 °C. Representative slices in the F1 dimension are displayed of the NOE's arising from the (C) AH_8 proton (8.3 ppm) and the (D) TH_6 proton (7.2 ppm) of dTdA to more clearly show the magnitude of the NOE intensities and the signal to noise ratio arising from the data collected. The peaks labeled E are NOE's from protons of the enzyme (see footnote 2).

to repeat the lower mixing time points to obtain reliable results since these data, which are critical for the extrapolation to zero mixing time, have the lowest signal to noise ratio. When distances from volume integration are compared to those from area integration, only the largest calculated distances (TH_6 → $TH_{5'}H_{5''}$), resulting from the smallest NOE, deviate significantly. Thus, volume integration is useful for obtaining accurate values for long distances. On comparing Tables III and IV, it is seen that the presence of the metal ion has significantly altered 4 of the 17 interproton distances, indicating different substrate conformations in the binary enzyme–dTdA and ternary enzyme–metal–dTdA complexes.

Conformation of Enzyme-Bound dTdA in the Presence of Metal Ion. The substrate conformation in the ternary E–M–S complex is described first since it is the one better determined. Using the 7 measured and 9 lower limit Co^{2+}–nucleus distances (Table II) together with the 17 measured (Table III) and 108 lower limit interproton distances (between which NOE's were

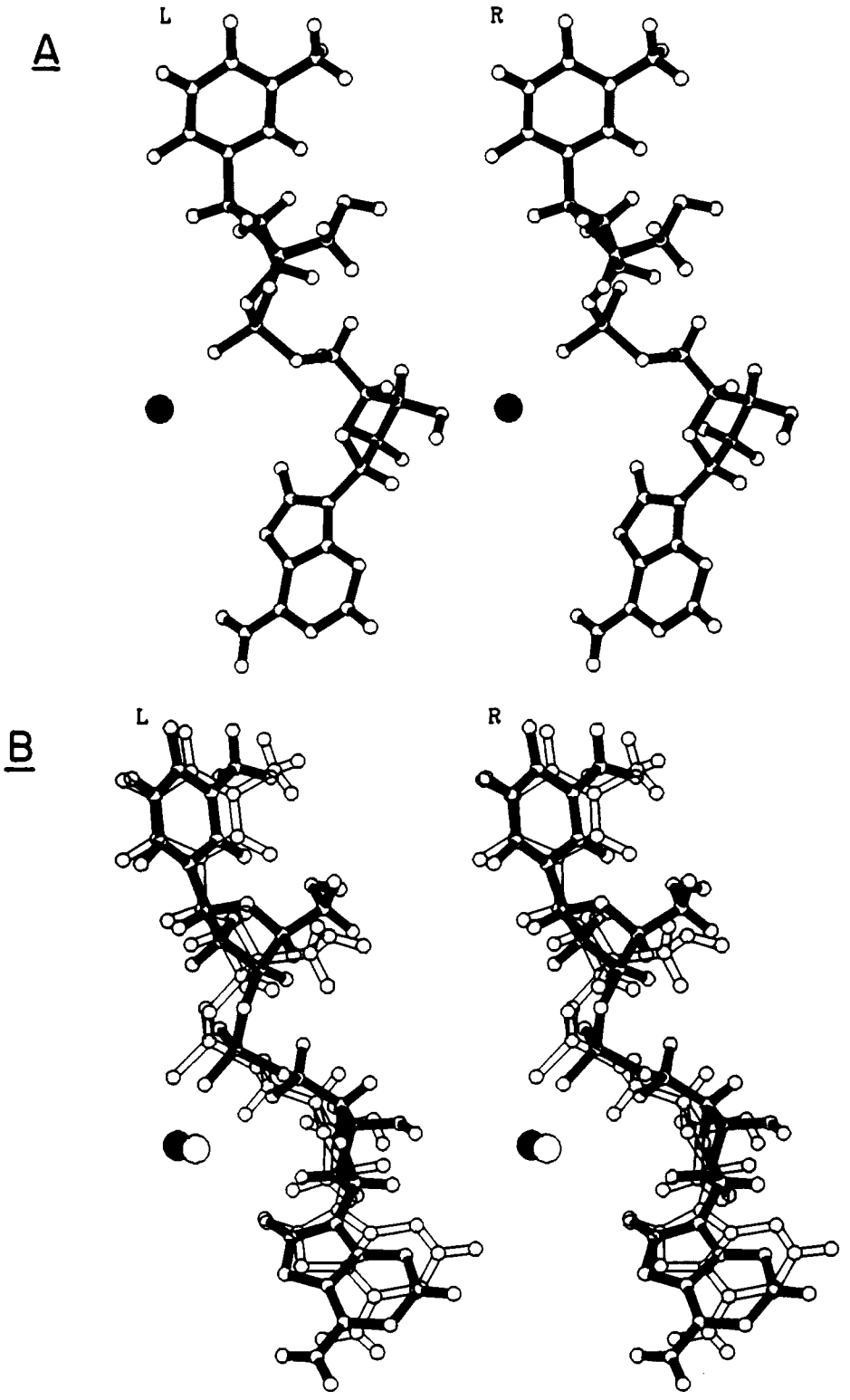

FIGURE 8: Computed conformations of enzyme-bound dTdA in the presence of metal ion based on the experimental distances of Tables II and III. (A) Best-fit conformation shown as stereo pair. (B) Comparison of the two most different acceptable conformations as stereo pairs showing the range of solutions. In (B), the root mean square difference between the two limiting structures is 1.08 Å.

not observed), a structural model of enzyme-bound dTdA, a molecule with 64 atoms, was computed. The computation was performed with use of the distance geometry method, D-Space, which takes into account the experimental distances and their errors as well as the van der Waals radii of the atoms of dTdA. Forty conformational searches, each starting from randomized coordinates, led to four structures that satisfied the experimental distances with a total deviation ≤0.64 Å and showed a total van der Waals overlap ≤0.55 Å. These four structures were found to be very similar. Figure 8A shows the structure that best fits the data, deviating by 0.42 Å from the measured distances and a by total van der Waals overlap of 0.51 Å. Figure 8B superimposes the two most different acceptable structures, illustrating the uniqueness of the solution. The structures in parts A and B of Figure 8 are consistent with one of the four models on the basis of distances to Co^{2+} alone. The conformational angles and their ranges for dTdA bound to staphylococcal nuclease in the presence of metal ions (Figure

Table V: Comparison of Dihedral Angles in Degrees of dTdA in the Enzyme–Metal–dTdA and Enzyme–dTdA Complexes of Staphylococcal Nuclease to A-, B-, and Z-DNA

torsional angle[a]	A-DNA	B-DNA	Z-DNA purines	Z-DNA pyrimidines	E–M–dTdA[c] dT	E–M–dTdA[c] dA	E–dTdA[d] dT	E–dTdA[d] dA
α	197 ± 12	316 ± 3	70 ± 22	var[b]		235 (193–235)		183 (132–190)
β	179 ± 6	var[b]	198 ± 23	193 ± 28		182 (172–186)		86 (85–87, 128–177)
γ	53 ± 11	37 ± 1	176 ± 19	57 ± 4	53 (33–53)	162 (157–170)	124 (120–132)	116 (116–143, 236–267)
δ	85 ± 12	120 ± 38	113 ± 37	143 ± 5	144 (130–144)	143 (142–143)	125 (108–141)	151 (151–162)
ϵ	204 ± 10	191 ± 36	218 ± 38	266 ± 9	198 (198–205)		67 (67, 199–209, 275–276)	
ζ	287 ± 5	127 ± 31	var[b]	var[b]	83 (67–83)		206 (119–140, 156–196, 206–244)	
χ	25 ± 14	67 ± 22	250 ± 19	17 ± 17	64 (64–73)	68 (66–68)	61 (57–76)	90 (84–112)

[a] Definition and values of torsional angles for A-, B-, and Z-DNA have been given previously (Saenger, 1983; Sunderalingam, 1973; Dickerson et al., 1982). Torsional angles are defined as follows: α, O_3'-P-O_5'-C_5'; β, P-O_5'-C_5'-C_4'; γ, O_5'-C_5'-C_4'-C_3'; δ, C_5'-C_4'-C_3'-O_3'; ϵ, C_4'-C_3'-O_3'-P; ζ, C_3'-O_3'-P-$O_5'_{(n+1)}$; χ_{dT}, O_4'-C_1'-N_1-C_6; χ_{dA}, O_4'-C_1'-N_1'-C_8. [b] In these cases the angles were variable in the several DNA samples measured (Saenger, 1983). [c] The angles reported were derived from the best acceptable structure with the lowest mean deviations from experimentally measured distances (0.3 Å). The errors reported include the range of measured angles in the four best structures with mean deviations ≤ 0.5 Å. [d] The angles reported were from the best acceptable structure with the lowest mean deviations from experimentally measured distances (0.2 Å). The errors reported include the entire range of measured angles in the 11 best structures with mean deviations ≤ 0.3 Å.

8) are summarized in Table V and compared with those for standard DNA conformations. The glycosidic torsional angles are high-anti for both the thymidine ($64° \leq \chi \leq 73°$) and deoxyadenosine nucleosides ($66° \leq \chi \leq 68°$). The $C_{5'}$-$C_{4'}$-$C_{3'}$-$O_{3'}$ exocyclic torsional angle, δ, provides a quantitative description of the sugar pucker (Levitt & Warshal, 1978; Dickerson et al., 1982). The δ value of 130–144° for thymidine and the values of 142–143° for deoxyadenosine (Table V) indicate that the sugar is predominantly C-2′-endo for both residues. While the individual nucleotides of dTdA resemble those of B-DNA when χ and δ are considered (Table V), the torsional angles α and γ of dA and ζ of dT, as well as the absence of any base stacking (Figure 8), argue against a B-DNA conformation. Similarly, A- and Z-conformations for enzyme-bound dTdA are easily ruled out. The highly extended structure for the enzyme-bound dTdA in the ternary E–M–S complex is consistent with the preference of staphylococcal nuclease for single-stranded DNA as a substrate (Cuatrecasas et al., 1967a).

Conformation of Enzyme-Bound dTdA in the Absence of Metal Ion. In forming the active ternary E–Ca^{2+}–DNA complex of staphylococcal nuclease two kinetic pathways are operative: one in which the metal binds first and the other in which the DNA binds first (Serpersu et al., 1986; Mildvan & Serpersu, 1989). Hence, the binary enzyme–dTdA complex is on the kinetic pathway leading to the active ternary complex. The conformation of dTdA in the binary enzyme–dTdA complex was studied by the NOESY method as described above for the ternary complex, and the resulting distances are summarized in Table IV.

Seventy computer searches of the conformation of dTdA in the binary enzyme–substrate complex, based on 13 measured (Table IV) and 112 lower limit interproton distances, led to 11 acceptable structures with total deviations ≤ 0.05 Å from the experimental data and with total van der Waals overlap of ≤0.11 Å. Figure 9A shows the structure that best fits the data, deviating by 0.03 Å from the measured distances, with a total van der Waals overlap of 0.05 Å. Figure 9B shows the two most different acceptable structures, and Table V summarizes the conformational angles and their ranges. In the acceptable structures, the conformational angles χ and δ are well determined, leading to a high-anti-O-1′-endo, C-2′-endo conformation for dT, and a high-anti-C-4′-endo, C-3′-exo conformation for dA. However, most of the conformational angles around the phosphorus are not well defined by the interproton distances alone (Figure 9B, Table V). Thus, the angles ϵ and ζ for dT show three alternative ranges of values, and the angles β and γ for dA show two alternative ranges (Table V). These uncertainties are expected since, in an unstacked DNA structure, no NOE's between the nucleotides were measurable and no metal to proton or metal to phosphorus distances were available to better define the phosphodiester region of dTdA. Despite these uncertainties, a significant difference exists in the structure of dTdA in the binary enzyme–dTdA complex from that in the ternary enzyme–metal–dTdA complex. This difference is indicated by the greater distances from $TH_{1'}$ to $TH_{4'}$, TH_6 to $TH_{2''}$, $AH_{1'}$ to $AH_{4'}$, and AH_8 to $AH_{3'}$ in the absence of metal (Tables III and IV) and by significantly different values of the conformational angles γ and ζ for dT and α, γ, δ, and χ for dA (Table V). Metal-induced differences in the angles ζ and α, which are on either side of the phosphorus, are reasonable since the metal coordinates an oxygen of the phosphodiester group (Table II). Metal-induced differences in the angles γ, δ, and χ for the leaving group dA are of interest, suggesting that the formation of the ternary E–M–S complex distorts the leaving group. These metal-induced effects may contribute to catalysis.

The use of Co^{2+} and La^{3+} as paramagnetic and diamagnetic metal ions, respectively, to determine the structure of the enzyme-bound substrate might be criticized since these metal ions do not activate the enzyme. However, these metal ions bind competitively at the Ca^{2+} site (Figure 3, Table I), and the dissociation constants of the enzyme–Co^{2+} and enzyme–Co^{2+}–dTdA complexes are very similar to those of Ca^{2+} (Table I), suggesting similar active site structures. While the dissociation constants of the La^{3+} complexes are lower than those of Ca^{2+}, probably due to the higher charge of La^{3+}, the structure of the enzyme–La^{3+}–pdTp complex is very similar to that of the enzyme–Ca^{2+}–pdTp complex as found in preliminary phase-sensitive NOESY spectra of the La^{3+} complex. The chemical shifts of the upfield methyl resonances and of all of the proton resonances of the aromatic residues of the enzyme–La^{3+}–pdTp complex show little or no differences (≤0.06 ppm) from those of the corresponding Ca^{2+} complex (Torchia et al., 1989; Wang et al., 1990). The inability of Co^{2+} or La^{3+} to activate staphylococcal nuclease may be due to the smaller ionic radius of Co^{2+} (0.72 Å) as compared to Ca^{2+} (0.99 Å) and the additional positive charge of La^{3+}.

Conclusions

As previously found with dinucleotides and with other small

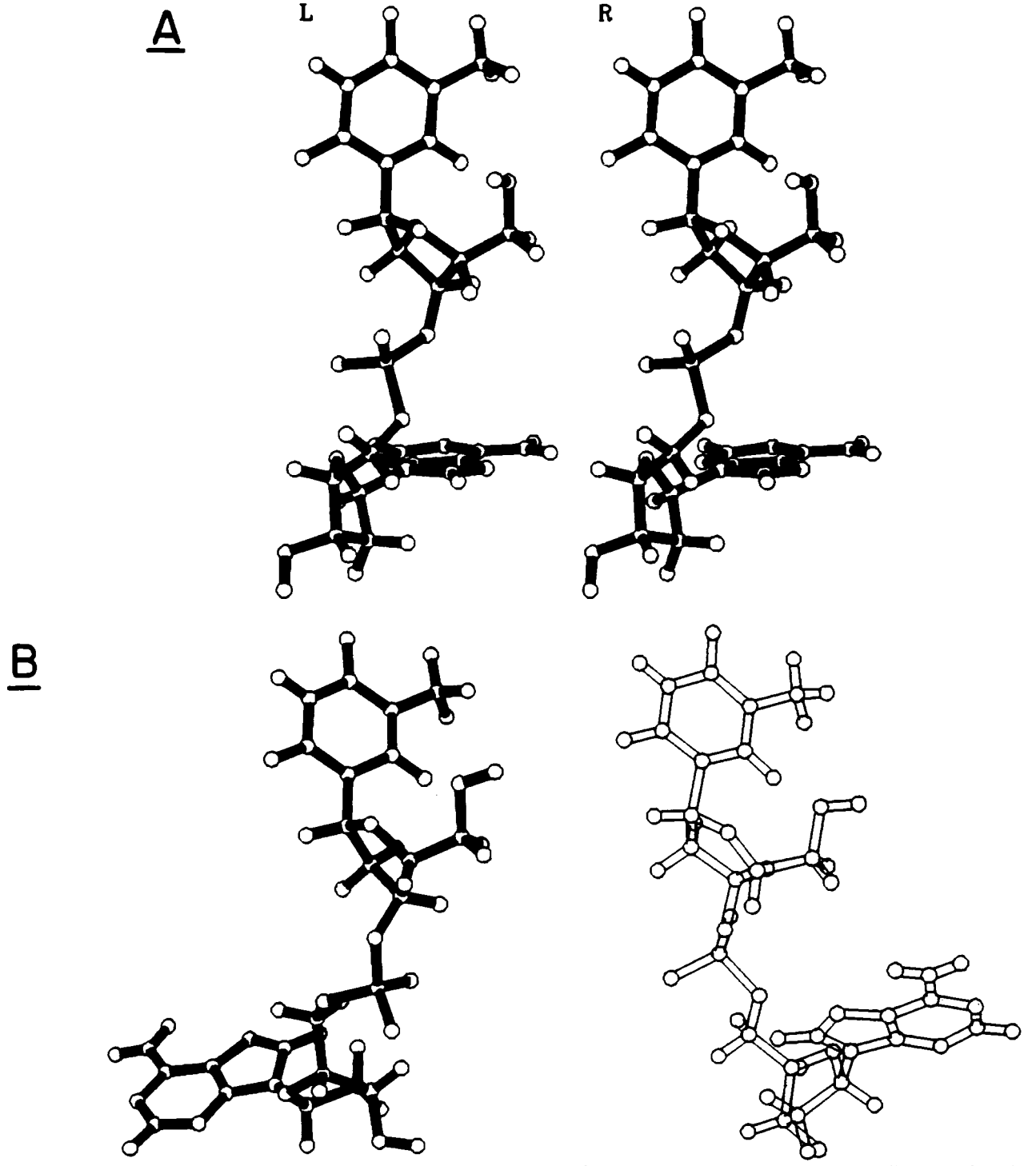

FIGURE 9: Computed conformations of enzyme bound dTdA in the absence of metal ions based on the experimental distances of Table IV. (A) Best-fit conformation shown as stereo pair. (B) The two most different acceptable conformations showing the range of solutions. In (B), the root mean square difference between the two limiting structures is 3.26 Å.

substrates, dTdA is a slow substrate of staphylococcal nuclease with a k_{cat} (2.5×10^4)-fold lower than that of single-stranded DNA. Paramagnetic effects of Co^{2+} on the relaxation rates of phosphorus and protons of dTdA establish rapid binding to and dissociation of the substrate from the ternary E–Co^{2+}–dTdA complex and yield 7 metal–nucleus and 9 lower limit metal–nucleus distances. The long Co^{2+} to phosphorus distance of 4.1 ± 0.9 Å, which is consistent with either a distorted inner sphere phosphoryl complex or the rapid averaging of 18% inner sphere and 82% second sphere coordination, may explain the reduced catalytic activity with dinucleotide substrates.

The distances from Co^{2+} alone were insufficient to uniquely define the conformation of enzyme-bound dTdA, as were 18 interproton distances and 108 lower limit interproton distances alone, as determined by time-dependent NOESY spectra. The combination of both sets of distances, however, yielded a very narrow range of conformations for dTdA in the ternary enzyme–metal–dTdA complex. Although the individual nucleosides of bound dTdA showed high-anti glycosidic torsional angles and C-2′-endo deoxyribose puckers as are found in B-DNA, the overall structure was highly extended with no base stacking, ruling out the B-, A-, or Z-conformations. This finding provides a structural explanation of the preference of

the enzyme for single-stranded DNA as substrate.

The binary enzyme–dTdA complex is on one of the two kinetic pathways leading to the active ternary E–M–S complex. The conformation of dTdA in the binary complex, while not uniquely determined by interproton distances, differs significantly from that found in the ternary enzyme–metal–dTdA complex. A comparison of the conformations of dTdA in the binary and ternary complexes indicates that the metal induces changes in conformation both at the attacked phosphorus and at the deoxyadenosyl leaving group of the enzyme-bound substrate. Both of these effects may contribute to catalysis.

Acknowledgments

We are grateful to Nikola Pavletich for advice on the use of the program Pluto and to Peggy Ford for secretarial assistance.

Registry No. dTdA, 19192-40-6; CO, 7440-48-4; Ca, 7440-70-2; Mn, 7439-96-5; La, 7439-91-0; staphylococcal nuclease, 9013-53-0.

References

Andersen, N. H., Eaton, H. L., & Lai, X. (1989) *Magn. Reson. Chem. 27*, 515–528.

Anfinsen, C. B., Cuatrecasas, P., & Taniuchi, H. (1971) *Enzymes (3rd Ed.) 4*, 177–204.

Baleja, J. D., Moult, J., Sykes, B. D. (1990) *J. Magn. Reson. 87*, 375–384.

Bean, B. L., Koren, R., & Mildvan, A. S. (1977) *Biochemistry 16*, 3322–3333.

Bradford, M. M. (1976) *Anal. Biochem. 72*, 248–254.

Carr, H. Y., & Purcell, E. M. (1954) *Phys. Rev. 94*, 630–638.

Chaiken, I. M., & Sanchez, G. R. (1972) *J. Biol. Chem. 247*, 6743–6747.

Cohn, M., & Townsend, J. (1954) *Nature (London) 173*, 1090–1091.

Cotton, F. A., Hazen, E. E., & Legg, M. J. (1979) *Proc. Natl. Acad. Sci. U.S.A. 76*, 2551–2555.

Cuatrecasas, P., Fuchs, S., & Anfinsen, C. B. (1967a) *J. Biol. Chem. 242*, 1541–1547.

Cuatrecasas, P., Fuchs, S., & Anfinsen, C. B. (1967b) *J. Biol. Chem. 242*, 3063–3067.

Cuatrecasas, P., Fuchs, S., & Anfinsen, C. B. (1967c) *J. Biol. Chem. 242*, 4759–4767.

Cuatrecasas, P., Wilchek, M., & Anfinsen, C. B. (1969) *Biochemistry 8*, 2277–2284.

Dickerson, R. E., Drew, H. R., Conner, B. N., Wing, R. M., Frantini, A. V., & Kopka, M. L. (1982) *Science 216*, 475–485.

Dunn, B. M., & Chaiken, I. M. (1975) *Biochemistry 14*, 2343–2351.

Dunn, B. M., DiBello, C., & Anfinsen, C. B. (1973) *J. Biol. Chem. 248*, 4769–4774.

Ferrin, L. J., & Mildvan, A. S. (1985) *Biochemistry 24*, 6904–6913.

Hibler, D. W., Stolowich, J. N., Reynolds, M. A., Gerlt, J. A., Wilde, J. A., & Bolton, P. H. (1987) *Biochemistry 26*, 6278–6286.

Jeener, J., Meier, B. H., Bachmann, P., & Ernst, R. R. (1979) *J. Chem. Phys. 71*, 4546–4553.

Kumar, A., Wagner, G., Ernst, R. R., & Wüthrich, K. (1980) *Biochem. Biophys. Res. Commun. 96*, 1156–1163.

Levitt, M., & Warshal, A. (1978) *J. Am. Chem. Soc. 100*, 2607–2617.

Loll, P. J., & Lattman, E. E. (1989) *Proteins: Struct., Funct., Genet. 5*, 183–201.

Marion, D., & Wüthrich, K. (1983) *Biochem. Biophys. Res. Commun. 113*, 967–974.

Mikulski, A. J., Sulkowski, E., Stasiuk, L., & Laskowski, M., Sr. (1969) *J. Biol. Chem. 244*, 6559–6565.

Mildvan, A. S., & Cohn, M. (1966) *J. Biol. Chem. 241*, 1178–1193.

Mildvan, A. S., & Engle, J. L. (1972) *Methods Enzymol. 26C*, 654–682.

Mildvan, A. S., & Gupta, R. K. (1978) *Methods Enzymol. 49G*, 322–359.

Mildvan, A. S., & Serpersu, E. H. (1989) in *Metal Ions in Biological Systems* (Sigel, H., Ed.) Vol. 25, pp 309–334, Marcel Dekker, Inc., New York.

Mildvan, A. S., Granot, J., Smith, G. M., & Liebman, M. (1979) *Adv. Inorg. Biochem. 2*, 211–236.

Reed, G. H., Cohn, M., & O'Sullivan, W. J. (1970) *J. Biol. Chem. 245*, 6547–6552.

Rosevear, P. R., & Mildvan, A. S. (1989) *Methods Enzymol. 177*, 333–375.

Rosevear, P. R., Bramson, H. N., O'Brian, C., Kaiser, E. T., & Mildvan, A. S. (1983) *Biochemistry 22*, 3439–3447.

Saenger, W. (1986) *Principles of Nucleic Acid Structure*, Springer-Verlag, New York.

Serpersu, E. H., Shortle, D., & Mildvan, A. S. (1986) *Biochemistry 25*, 68–77.

Serpersu, E. H., Shortle, D., & Mildvan, A. S. (1987) *Biochemistry 26*, 1289–1300.

Serpersu, E. H., McCracken, J., Peisach, J., & Mildvan, A. S. (1988) *Biochemistry 27*, 8034–8044.

Serpersu, E. H., Hibler, D. W., Gerlt, J. A., & Mildvan, A. S. (1989) *Biochemistry 28*, 1539–1548.

Shortle, D., & Meeker, A. K. (1989) *Biochemistry 28*, 936–944.

Solomon, I., & Bloembergen, N. (1956) *J. Chem. Phys. 25*, 261–266.

Sulkowski, E., & Laskowski, M., Sr. (1970) *Biochim. Biophys. Acta 217*, 538–540.

Sundaralingam, M. (1973) *Jerusalem Symp. Quantum Chem. Biochem. 5*, 417–456.

Torchia, D. A., Sparks, S. W., & Bax, A. (1989) *Biochemistry 28*, 5509–5524.

Tucker, P. W., Hazen, E. E., Jr., & Cotton, F. A. (1978) *Mol. Cell. Biochem. 23*, 67–86.

Wang, J., LeMaster, D. M., & Markely, J. L. (1990) *Biochemistry 29*, 88–101.

Weber, D. J., Lebowitz, M. S., & Mildvan, A. S. (1990a) *FASEB J.*, A1979.

Weber, D. J., Serpersu, E. H., Shortle, D., & Mildvan, A. S. (1990b) *Biochemistry 29*, 8632–8642.

Weber, D. J., Meeker, A. K., & Mildvan, A. S. (1991) *Biochemistry* in press.

Wüthrich, K. (1986) *NMR of Proteins and Nucleic Acids*, Wiley, New York.